Real Potential in Alpha-Nucleus Scattering*

P. Mailandt, J. S. Lilley, and G. W. Greenlees
Department of Physics, University of Minnesota, Minneapolis, Minnesota 55455
(Received 10 November 1972)

Measurements of α-nucleus elastic differential-cross-section data at 27 MeV from ^{45}Sc, ^{65}Cu, ^{90}Zr, and ^{122}Sn, over the angular range 15 (×2.5) to 175° are reported. The data are analyzed using both a standard six-parameter optical model and a folding model. The latter uses an effective nucleon-α interaction obtained from a global analysis of free nucleon-α scattering data below 12 MeV incident nucleon energy which is folded with a nuclear matter distribution to obtain the real part of the α-nucleus potential. The fits with the folding model are improved appreciably over those obtained using the standard optical model and are sensitive to the choice of matter parameters. The matter mean-square radii deduced are in good agreement with other estimates.

I. INTRODUCTION

The study of the elastic scattering of α particles by atomic nuclei has received extensive and continuous attention in nuclear physics from the very beginnings of the subject. The differential-cross sections observed at forward angles and at energies above the Coulomb barrier exhibit strong diffraction-like patterns which are well represented in terms of a model corresponding to a strongly absorbing sphere.[1] With the advent of more accurate and extensive data, more sophisticated models were needed to represent the data and current phenomenological analyses use an optical-model description with either four or six parameters.[2] However, when the differential-cross-section measurements extend into the backward hemisphere, such models using Woods-Saxon form factors have difficulty in simultaneously reproducing both the forward- and backward-angle data.[3] In some cases a variety of special mechanisms have been proposed to account for the details of the scattering at backward angles.[4]

In parallel with this development of phenomenological models for the reaction, numerous attempts have been made to give a more microscopic description of elastic α-nucleus scattering using an effective interaction for the real potential. The interactions used have corresponded either to a nucleon-nucleon interation,[5,6] or to a nucleon-α interaction.[7] The imaginary potential has been either taken to have the same form as the folded real potential or has been parametrized independently. In general these studies have used parametrized Yukawa or Gaussian forms for the effective interaction and have demanded only a qualitative or semiquantitative representation of the scattering data at forward angles. However, Budzanowski *et al.*[6] using various nucleon-nucleon effective interactions with Fermi-shaped nuclear matter distributions for both the nucleus and the α particle, compared their calculations with ^{59}Co(α, α) data at 27.5 MeV over a wide angular range (15–179°). The main features of the data at backward angles were well reproduced by the calculations, but in other angular regions sizable differences were found, although the periodicities of the data were reproduced.

In some cases, the effective nucleon-nucleon interaction obtained in these studies has been compared to ones obtained for the free nucleon-nucleon interaction. However, little attention has been paid as to how well the nucleon-nucleon interaction folded into the matter distribution of the α particle, or the nucleon-α interaction itself, if it was used directly, reproduce existing nucleon-^{4}He scattering data. A reasonable representation of such data would seem to be a necessary requirement if such procedures are to be anything other than an alternative phenomenological representation of the α-nucleus interaction. Batty, Friedman, and Jackson[8] examined this point for published effective interactions and found that they had only limited success in reproducing the nucleon-^{4}He data. These authors were able to specify the acceptable limits on the parameter values of a Gaussian nucleon-α effective interaction, which would reproduce the observed α-nucleus scattering in the forward-angle region, and their results indicated that the effective interaction which gave the best fits also came closest to reproducing the nucleon-α phase shifts.

The present paper reports measurements of the elastic scattering of α particles at about 27 MeV (lab) from four nuclei. The data are relatively accurate and cover the angular range from 15 to 175°. The data are analyzed using both a phenomenological optical model and a folding model with

an effective nucleon-α interaction. The folding model gives a much improved representation of the α-nucleus data, over the whole angular range, compared to the standard optical model and with fewer parameters. In addition, the nucleon-α interaction gives an excellent representation of published nucleon-^{4}He data. The quality of fit obtained to α-nucleus data, is sensitive to the choice of parameters for the matter distribution of the nucleus; the best fits are obtained with a choice consistent with current best estimates of these parameters. A preliminary account of this work has been published previously.[9]

II. EXPERIMENTAL PROCEDURE

Beams of 27- MeV α particles from the Minnesota MP tandem were used for the present measurements. The spectra of particles scattered from foil targets at the center of a "2.5-m" scattering chamber were recorded via surface-barrier detectors.

The scattering chamber consisted of a 45-cm-diam cylindrical body to which was attached a wedge-shaped snout, covering a 32° angular range, which enabled detectors to be placed up to 120 cm from the target. The snout and body could be rotated under vacuum via a sliding seal attached to the beam input tube. Magnetically shielded Faraday cups for beam integration were available at 20° intervals. The angular range accessible to detectors placed in the snout, was −12 to +165°. The snout housed a detector cart which could be positioned remotely via a stepping motor and gear mechanism operating along the arc of a circle centered on the target. The steps correspond to movements of 0.1° with the assembly placed at 60 cm from the target. Detector positioning using this device was accurate to better than 0.02°. Measurements between 15 and 165° were taken with an array of four surface-barrier detectors mounted on the cart assembly with separations of 5°. Measurements at angles beyond 165° were made using two surface-barrier, position-sensitive detectors (1 × 3 cm, 600-μm thick). These were placed on either side of the beam line in the main body of the chamber and covered angular ranges 167–175° and 165–170°, respectively. The position signal from these detectors enabled the recorded counts to be routed into bins corresponding to a 1° angular acceptance at 1° intervals between 162 and 175°. The energy signal was corrected for kinematic spread using computer software, in order to facilitate a clean separation of the elastic peak. The position linearity of these detectors was better than 1% but the differential-position linearity varied by as much as 40% across a detector. Such a variation, in the present application, is reflected directly in the cross-section determination. A correction therefore was applied via a calibration of the detectors using the elastic scattering from a thin Bi target at forward angles (35–43°) and 20-MeV incident energy, where the Rutherford scattering law was known to be valid. A given detector proved to have a stable calibration and the over-all arrangement proved very satisfactory in operation.

Two detectors, placed at ±30° relative to the beam direction, served to monitor continuously the beam position on the target. The beam passing

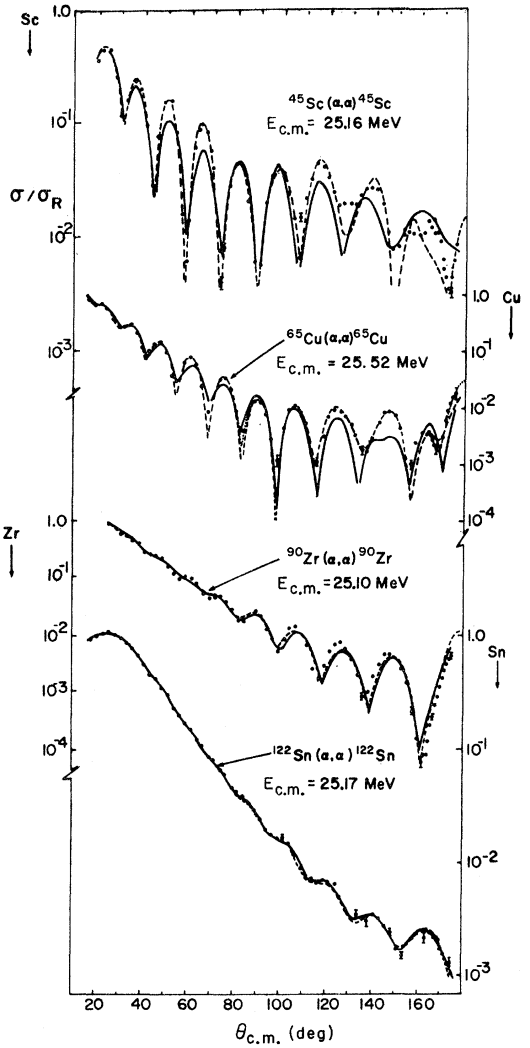

FIG. 1. Angular distributions for elastic α-nucleus scattering. The points are experimental data; the full lines are the best fit predictions using a standard six-parameter optical model; the broken lines are the best fit predictions using the folding model with either four (- - -) or six (· · ·) parameters. The corresponding parameter and χ^2 values are given in Table I.

through the target was collected in a Faraday cup and integrated. A comparison of the summed counts in the two monitor detectors with the integrated beam, provided a check of any changes in the effective target thickness. Relative-cross sections were obtained by normalizing the counting rate to the monitor detectors and the absolute normalization was obtained using forward-angle measurements from the targets using 7-MeV α beams and assuming these obeyed a Rutherford scattering law. The results for the position-sensitive detectors were normalized to the cart-detector data by taking measurements with both arrangements at about 120°.

Self-supporting targets, about 1 mg/cm^2 thick, of ^{45}Sc, ^{65}Cu, ^{90}Zr, and ^{122}Sn were used in the present work. Using the cart detectors, measurements were taken at 2.5° intervals from 15 to 165°; the angular acceptance of these detectors was ±0.25° and the absolute angular positioning was estimated to be accurate to better than 0.1°. An over-all energy resolution of ±60 keV was typical and the measured-cross sections were estimated to have an absolute accuracy of between ±2 and ±5% except for a few points at deep minima in the angular distributions. Using the position sensitive detectors (162–175°) an energy resolution of 150 keV was typical; cross sections were recorded every 1° with an angular acceptance of ±0.5° and an absolute accuracy of ±8%. The experimental data points for the different cases are included in Fig. 1.

For each target, excitation functions were taken in 100-keV steps for a number of scattering angles in the backward hemisphere. In all cases, smooth variations were found with no evidence for resonance-like structure which might invalidate the approach used in the present analysis.

III. ANALYSIS

A. Standard Optical Model

When data covering a wide angular range are available, as in the present case, it has been found[2] that a six-parameter optical-model potential is needed to give a good representation of the data. Such a potential therefore was used in the present analysis and had the form

$$V(r) = V_C(r) - V_R f(r, r_R, a_R) - iW_V f(r, r_I, a_I), \tag{1}$$

where

$$f(r, r_0, a_0) = [1 + \exp(r - r_0 A^{1/3})/a_0]^{-1}$$

and $V_C(r)$ is the Coulomb potential due to a nuclear charge distribution of the form $f(r, r_C, a_C)$ with[10] $r_C = (1.106 + 1.05 \times 10^{-4} A)$ and $a_C = 0.502$ fm. The data for the different elements were fitted using this potential and the computer code RAROMP.[11] The parameters of the model, V_R, r_R, a_R, W_V, r_I, and a_I, were varied to find a minimum in χ^2 defined by:

$$\chi^2 = \frac{1}{N} \sum_{i=1}^{N} \left[\frac{\sigma_{th}(\Theta_i) - \sigma_{exp}(\Theta_i)}{\Delta\sigma_{exp}(\Theta_i)} \right]^2 \tag{2}$$

where N is the number of data points and $\sigma_{th}(\Theta_i)$, $\sigma_{exp}(\Theta_i)$, and $\Delta\sigma_{exp}(\Theta_i)$ are the model value, the experimental value and the error in the experimental value, respectively, of the differential-cross sections at angle Θ_i.

An extensive investigation of the six-parameter space was carried out and all of the well-known parameter ambiguities were found. A detailed account of this investigation will not be presented here since it provided no particularly novel insights into the application of the optical model to elastic α-nucleus scattering. In general, no unique parameter-search sequence was found which was satisfactory in all circumstances and for all families of parameter sets. A variety of search sequences were used along with gridding procedures to map out the χ^2 contours. For each element, several parameter sets were found which did equally well in representing the data; these, in general, had r_R values between 1.3 and 1.5 fm and did appreciably better in representing the data at forward angles (<90°) than at backward angles (>90°). As was found in Ref. 3, parameter sets with $r_R \sim 1.1$ fm could be found which gave improved fits at backward angles, but the over-all χ^2 values in these cases were approximately a factor of 2 greater than the optimum values. Typical best fits obtained in the different cases are included in Fig. 1.

The parameter ambiguities are best illustrated by comparing plots of the real and of the imaginary potentials for the equivalent sets. Such plots are given in Fig. 2. For each nucleus, the tail regions of the equivalent-real-central potentials are very similar and have a common point at radial distances between 8 and 10 fm. These cross-over points of the equivalent-real potentials are at distances (R_X) close to the strong absorption radii. The strong absorption radius has been used by other authors[12] to characterize elastic α scattering and is the classical turning point for a particle with angular momentum L corresponding to $\mathrm{Re}(\eta_L) = \frac{1}{2}$, where η_L is the reflection coefficient.

In two cases, ^{45}Sc and ^{65}Cu (Fig. 2), the imaginary potentials for equivalent parameter sets show similar features to the real potential though with a common point radial distance about 2 fm

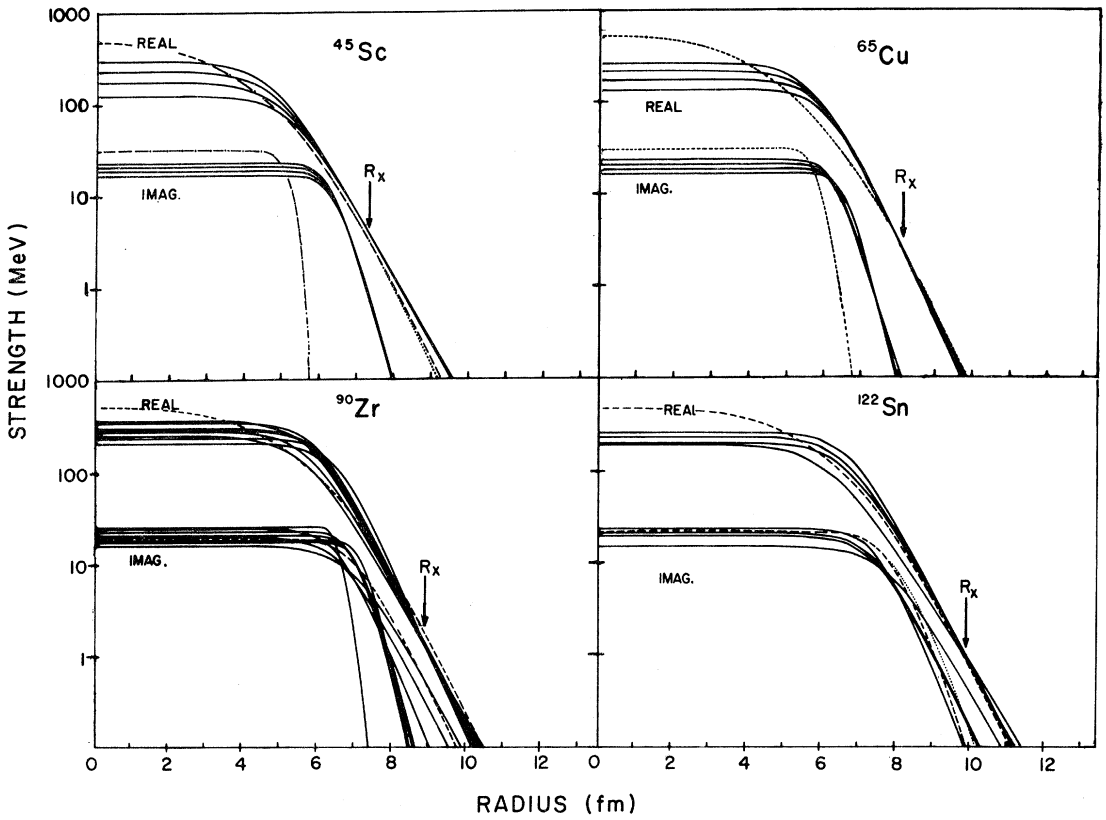

FIG. 2. Radial distributions of the real and imaginary potentials found to yield best fits to the α-nucleus elastic scattering data. The full lines correspond to equivalent sets found using the standard six-parameter optical model and the broken lines to the best fits using the folding model.

smaller. For ^{90}Zr and ^{122}Sn on the other hand, wide variations are seen in the shapes of the equivalent imaginary potentials. However, the ^{90}Zr and ^{122}Sn angular distributions (Fig. 1) show considerably less structure than do those of ^{45}Sc and ^{65}Cu; in such cases the ill-defined nature of the imaginary potential has been noted previously.[2]

The importance of the tail region of the real potential in α elastic scattering has been reported by many authors[2] and implies that, when using a Woods-Saxon form for the potential, a_R is the only parameter which alone has any significance since it determines the slope of the tail of the potential. It is perhaps surprising in these circumstances, that alternative parametrizations of the potential which give more flexibility to the shape of the tail region, have not been investigated.

B. Folding Model

The positions of the crossover points in the equivalent real potentials of Fig. 2, occur at radial distances, R_X, approximately 4 fm beyond the half-density points of the corresponding nuclear distributions. This suggests that the important part of the real potential, for the present reaction, is determined by interactions taking place in regions of relatively low nucleon density. The finite range of the force involved will cause contributions to the potential at the crossover distance to come from regions of higher density, but, for typical ranges found in such work, the nucleon densities involved should not exceed 10% of the central value. Since the imaginary potential has a relatively small magnitude and the nucleon densities are low, it is not unreasonable to expect the real potential in the tail region to be reproduced reasonably well by the folding of a free nucleon-α interaction with the appropriate nuclear-nucleon distribution. Lilley[13] examined the plausibility of such an approach by comparing the magnitudes and slopes of the real-central potential at the crossover points, as reported in published elastic α-nucleus scattering analyses for ^{58}Ni and ^{208}Pb in the energy range 20–60 MeV,

with values computed from a folding of a Fermi-shaped matter distribution with a phenomenological potential known to fit nucleon-α-scattering data. Good agreement was found with matter distributions which were in agreement with other determinations.

The nucleon-α potential used by Lilley[13] was taken from an optical-model analysis of n-^{4}He and p-^{4}He data up to 20-MeV incident energy, by Satchler *et al.*[14] This analysis used a Woods-Saxon form for the real central potential and a Thomas form for the spin-orbit potential. The authors of Ref. 14 suggested that an improved representation of the data might be achieved using a global-computer program which simultaneously fitted the data at all energies. In the present section such a global analysis of nucleon-α data is reported and the resulting real-central potential, folded into the nuclear matter distribution for the different targets, is used to analyze the present α-nucleus data.

1. Analysis of Nucleon-^{4}He Data

The energy of the α particles at the points R_X (Fig. 2) are in the range 12–22 MeV. This corresponds to an energy range of 3–5.5 MeV for nucleons incident upon a helium target. The choice of p-^{4}He and n-^{4}He date for the present global analysis was determined by the availability of data at various energies and the need to include the energy range 3–5.5 MeV of laboratory nucleon energy. Data for neutrons[15] scattered by helium in the range 1.008 to 10.0 MeV were used along with data for protons[16] scattered by helium in the range 1.997 to 12.04 MeV. These data are included in Figs. 3 and 4.

The global code BOM[17] was used to analyze simultaneously the data sets to find a minimum

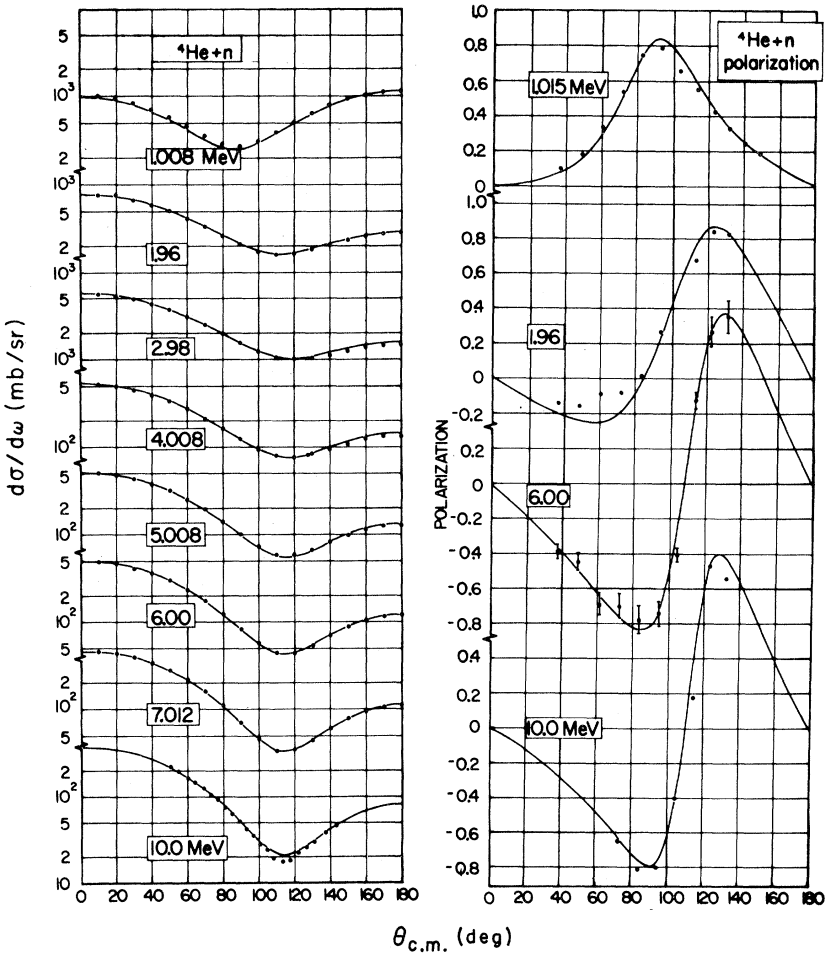

FIG. 3. Comparison of experimental points with model predictions for neutron-^{4}He elastic scattering data at various energies. The data are from Ref. 15 and the model predictions are from the present global analysis yielding the potential parameters of Eq. (4).

in the function

$$F = \sum_{n=1}^{n_{\max}} (\chi^2_\sigma + \chi^2_p),$$

where χ_σ^2 denotes χ^2 per point value of the differential-cross sections, $\sigma(\Theta)$, for the nth data set containing N_σ points; and χ_p^2 denotes χ^2 per point value for the polarization data, $P(\Theta)$, for the nth data set containing N_p points, with χ^2 as defined in Eq. (2). The search program thus weights each data set equally.

The results of Ref. 14 were used as a guide for a suitable choice of optical-model potential, which was of the form:

$$V(r) = V_C(r) - V_{RN} f(r, r_{RN}, a_{RN}) + \left(\frac{\hbar}{m_\pi c}\right)^2 V_{SN} \vec{l}\cdot\vec{\sigma} \frac{1}{r} f'(r, r_{SN}, a_{SN}) \quad (3)$$

with $V_C(r)$ being the Coulomb potential due to a uniformly-charged sphere of radius 2.06 fm and $f(r, r_0, a_0)$ as defined in Eq. (1). An imaginary term was not included since the energies involved in the analysis are below the reaction threshold.

After some preliminary searching, the parameters a_{RN} and a_{SN} were made equal and fixed at 0.34 fm and r_{SN} was set equal to 1.117 fm. Following Ref. 14 the parameters r_{RN} and V_{SN} were assumed to depend linearly upon the nucleon-bombarding energy and written as

$$r_{RN} = r_{RNO} + \beta E$$

and

$$V_{SN} = V_{SNO} + \gamma E.$$

The parameters V_{RN}, r_{RNO}, β, a_{RN}, V_{SNO}, and γ were varied to find a minimum in F for all the proton data sets and separately for all the neutron data sets. It was not possible to obtain the best representation for both the proton and the neutron data with the same parameter values. However, this was possible using the same central-potential parameters and different V_{SNO} and γ values for the two cases. In fitting the neutron data it was noticed that two of the polarization angular distributions ($E_n = 1.96$ MeV and $E_n = 6.00$ MeV) always gave a disproportionately large contribution to the F value. The errors associated with these data

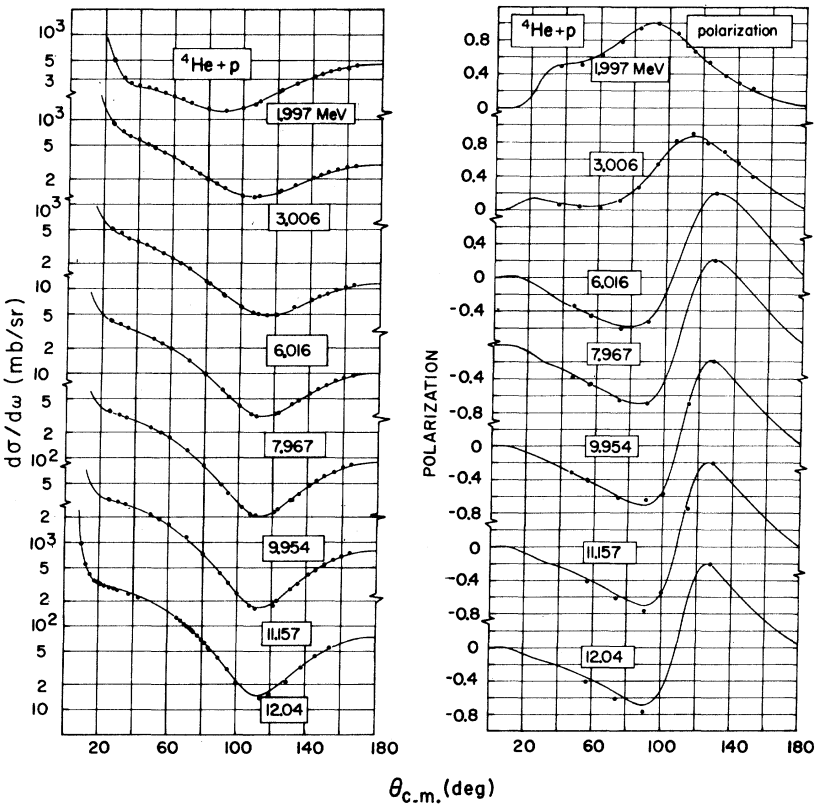

FIG. 4. Comparison of experimental points with model predictions for proton-^{4}He elastic scattering data at various energies. The data are from Ref. 16 and the model predictions are from the present global analysis yielding the potential parameters of Eq. (4).

were increased, therefore, to equalize approximately the contributions to F from the different data sets. Good fits were obtained using the following parameters for the nucleon-α interaction[18]:

$$V_{RN} = 42.5 \text{ MeV},$$
$$r_{RN} = (1.483 - 0.009E) \text{ fm},$$
$$a_{RN} = 0.34 \text{ fm},$$
$$V_{Sn} = (2.496 + 0.256\ E) \text{ MeV (neutrons)}, \quad (4)$$
$$V_{Sp} = (3.864 + 0.0316\ E) \text{ MeV (protons)},$$
$$r_{SN} = 1.117 \text{ fm},$$
$$a_{SN} = 0.34 \text{ fm},$$

with E being the laboratory nucleon energy in MeV. The energy dependence of the spin-orbit strength differs considerably for protons and neutrons; however, the magnitude of this term in the two cases is approximately the same in the middle of the energy range considered in the analysis.

The predictions given by the potential of Eq. (4) are compared with the data in Fig. 3 (neutrons) and Fig. 4 (protons). These figures show that a very good representation of the data has been achieved. The over-all quality of fit is slightly better than was achieved in Ref. 14, mainly because of a superior representation of the polarization data. Since the present parametrization constrains V_{RN} to be the same for neutrons and protons, whereas Ref. 14 allowed them to differ, the slightly improved representation of the data presented here justifies the global-analysis approach.

No extensive investigation was undertaken to search for alternative parametrizations of the potential which could possibly give an equivalent or superior representation of the data. However, it was confirmed that the energy dependence of the real-central potential could be included equally well in the strength parameter rather than in the radius parameter as in Eq. (4).

2. *Analysis of α-Nucleus Data*

The real-central-interaction potential $[V_{RF}(r)]$ for this analysis was obtained by a folding of the real part of the nucleon-α potential found in Sec. III B 1 [Eq. (4)] with the appropriate nuclear matter distribution. Thus[10]:

$$V_{RF}(r) = \int \rho_m(r') V_{N\alpha}(|\vec{r} - \vec{r}'|)\, d\vec{r}', \quad (5)$$

where $\rho_m(r')$, the nuclear matter distribution, was assumed to have the form

$$\rho_m(r') = [1 + \exp(r' - r_m A^{1/3})/a_m]^{-1}. \quad (6)$$

This folded potential replaces the real-central part of the standard optical-model potential $[V_R f(r, r_R, a_R)]$ in Eq. (1); the Coulomb and the imaginary-potential representation of Eq. (1) remain unchanged.

The radius parameter of $V_{N\alpha}$ is slightly energy-dependent; the energy chosen for a particular case corresponded to the energy for an interaction taking place at distances R_x (Fig. 2). This choice is not critical to the analysis.

(a) Fixed matter parameters. In the initial analysis it was assumed that the neutron and proton distributions of the nuclei investigated were identical. This is probably a reasonable assumption for all cases except ^{122}Sn where there is some evidence that the neutron size slightly exceeds the proton size.[19] Thus the r_m and a_m of Eq. (6) were set equal to the corresponding proton values (r_p, a_p). These r_p and a_p values were obtained from the work of Acker *et al.*[20] who investigated the μ-mesonic x-ray spectra of a range of nuclei ($Z = 17$ to 83). These authors deduced the rms radii of the charge distributions, $\langle r^2 \rangle_{ch}^{1/2}$, which are readily converted to the rms radii of the proton distribution via the relation

$$\langle r^2 \rangle_{ch} = \langle r^2 \rangle_p + 0.64, \quad (7)$$

taking 0.64 fm^2 to be the mean square radius of the proton-charge distribution. The nuclear proton rms radii for the present work were obtained by interpolation of the values obtained from the charge radii of Ref. 20 in this way. Acker *et al.* assumed the charge distributions to have the form of Eq. (6) for which:

$$\langle r^2 \rangle_{ch} = \tfrac{3}{5} r_{ch}^2 A^{2/3} + \tfrac{7}{5} (\pi a_{ch})^2.$$

These authors found that a charge diffuseness value $a_{ch} = 0.568$ fm to be a reasonable choice for all nuclei investigated. In the present work, it was assumed that $r_p = r_{ch}$ for each individual nucleus and that the difference in rms radii of the charge and proton distributions, corresponding to Eq. (7), could be ascribed to a change in diffuseness value, yielding $a_p = 0.52$ fm for all nuclei. The r_p $(= r_m)$ values thus obtained ranged from 1.02 to 1.081 fm and are included in Table I.

With the matter parameters fixed as described above, the four parameters $V_{RFO}(= |V_{RF}|_{r=0})$, W_V, r_I, and a_I were varied to find a minimum in χ^2 for each case. The results are included in Fig. 1; the corresponding parameter values are given in Table I, where the χ^2 values are compared with those found in the standard optical-model analysis of Sec. III A. With the exception of ^{122}Sn, the χ^2 values are lower using the four-parameter folding model than those obtained with the standard six-parameter optical model. For ^{45}Sc and ^{65}Cu, the reduction in χ^2 is about a factor of 2 and Fig. 1 re-

TABLE I. Parameter values obtained in standard optical model (S) and folding model (F) analyses of α-nucleus data. The proton rms radii are obtained from Ref. 20. R is the ratio of the folded strength to that predicted by the nucleon-α potential. In all cases the imaginary potentials (W_V, r_I, a_I) were varied. Strengths are in MeV. Lengths are in fm.

Nucleus	Model	Real parameter varied	V_{RFO}	r_m	a_m	W_V	r_I	a_I	χ^2	$\langle r^2\rangle_m^{1/2}$	$\langle r^2\rangle_p^{1/2}$	$\langle r^2\rangle_n^{1/2} - \langle r^2\rangle_p^{1/2}$	R
^{45}Sc	S	V_R, r_R, a_R				~20	~1.78	~0.31	61 – 66				
	F	V_{RFO}	477.2	1.020	0.520	31.06	1.446	0.177	37.3	3.42			1.08
	F	V_{RFO}, r_m, a_m	473.4	1.024	0.509	30.71	1.448	0.186	29.0	3.40	3.42 ± 0.1	−0.035 ± 0.09	1.07
^{65}Cu	S	V_R, r_R, a_R				~20	~1.6	~0.29	68 – 78				
	F	V_{RFO}	538.4	1.032	0.520	31.51	1.432	0.201	32.3	3.76			1.14
	F	V_{RFO}, r_m, a_m	506.3	1.080	0.473	30.11	1.444	0.184	17.65	3.796	3.76 ± 0.08	+0.065 ± 0.06	1.19
^{90}Zr	S	V_R, r_R, a_R				~21	~1.5	~0.3	26 – 37				
	F	V_{RFO}	452.4	1.073	0.520	18.68	1.562	0.521	20.8	4.20			0.996
	F	V_{RFO}, r_m, a_m	429.5	1.112	0.462	26.71	1.347	0.613	18.6	4.23	4.20 ± 0.1	+0.055 ± 0.25	1.017
^{122}Sn	S	V_R, r_R, a_R				~19	~1.51	~0.52	1.4 – 1.6				
	F	V_{RFO}	489.0	1.081	0.520	21.72	1.560	0.391	5.0	4.58			1.06
	F	V_{RFO}, r_m, a_m	458.5	1.108	0.535	21.34	1.583	0.450	1.24	4.70	4.58 ± 0.03	+0.20 ± 0.09	0.995

flects this with visually improved representations of the data. The increase in χ^2 associated with ^{122}Sn for the folding model is attributed to a breakdown in the assumption that the neutron and proton distributions are identical and is discussed later in this section.

The significant improvement in representation seen in Fig. 1, for ^{45}Sc and ^{65}Cu, using fewer parameters, is both somewhat surprising and encouraging and must be associated with the change in potential shape associated with the folding of two Woods-Saxon forms since the imaginary potential was parametrized identically and allowed to vary freely, as it was in the standard optical-model analysis (Sec. III A).

(b) Sensitivity to choice of matter parameters. The measurements from which the proton (and matter) parameters were obtained, only determine with any accuracy one size parameter of the charge (and proton) distribution which, for present purposes, is taken to be the rms radius.[21] In order to obtain a radial distribution, a functional form has to be assumed [Eq. (6)], with two parameters r_{ch} and a_{ch}, and a suitable choice made for one of them (a_{ch}). Therefore, it is reasonable to explore the effects of variations in the matter parameters on the representation of the present data, within a range consistent with the measured rms charge radii.

The analysis was repeated searching on the r_m and a_m values along with V_{RFO}, W_V, r_I, and a_I. The resulting parameter values are included in Table I and the predictions are included in Fig. 1. In the case of ^{45}Sc only small changes in the matter parameters (r_m, a_m, and $\langle r^2\rangle_m^{1/2}$) occur, with some improvement in the χ^2 values but with little change in the visual quality of the fit. For ^{65}Cu and ^{122}Sn a significant improvement in χ^2 is effected and, for ^{65}Cu, the visual fit is improved appreciably at large angles and the radius and diffuseness parameters show small but significant departures from the original proton values. However, the rms matter radius of ^{65}Cu shows little change and the new value is well within the error limits of the proton value derived from Ref. 20. For ^{122}Sn, the χ^2 improves by a factor of 4 to a value below that obtained with the standard model but the rms radius exceeds the rms proton radius by 4 times the error value of the latter. This suggests that in this case, the assumption of identical neutron and proton distributions is not valid and indicates a greater size for the neutrons.

It was decided to explore further the sensitivity of the model to the r_m and a_m values. In the case of ^{65}Cu this was done in some detail by finding χ^2 minima with variation of V_{RFO}, W_V, r_I, and a_I for a range of combinations of fixed values for

r_m and a_m. This enabled a χ^2 contour plot to be drawn in the r_m, a_m plane. This plot is shown in Fig. 5 where it is seen that within a given contour, the variation $\langle r^2\rangle_m^{1/2}$ is about one quarter of the variation of r_m and about one tenth of the variation of a_m. Taking a criterion of 1.5 times the optimum χ^2 as defining the acceptable range to produce a satisfactory representation of the data, gives values $\langle r^2\rangle_m^{1/2} = 3.796 \pm 0.024$ fm, $r_m = 1.080 \pm 0.022$ fm, and $a_m = 0.473 \pm 0.025$ fm.

The determination of plots such as Fig. 5 is time consuming and was not repeated in the other cases. Instead, χ^2 minima were found with variation of V_{RFO}, W_V, r_I, and a_I, for a range of values of r_m, at fixed a_m values. For ^{65}Cu and ^{90}Zr the a_m value for the best fit was chosen since these were appreciably different from the original values chosen in Sec. III 2 a. For the other two cases the original value $a_m = 0.52$ fm was used. Inspection of Fig. 5 shows that the width of such curves for a given χ^2 value will underestimate the spread in r_m.

Using the relationship:

$$A\langle r^2\rangle_m = Z\langle r^2\rangle_p + N\langle r^2\rangle_n ,$$

together with $\langle r^2\rangle_p$ deduced from Ref. 20, enables the $\langle r^2\rangle_m$ values to be converted into corresponding neutron rms radius values $\langle r^2\rangle_n^{1/2}$. The results are presented in Fig. 6 as a plot of χ^2 value against the neutron-proton rms radius difference $(\langle r^2\rangle_n^{1/2} - \langle r^2\rangle_p^{1/2})$. Taking the 1.5 $\chi^2_{\min}$ criterion as defining the acceptable limits, Fig. 6 shows that, in all cases except ^{122}Sn, the results are consistent with a neutron-proton rms radius difference of zero. For ^{122}Sn the difference is $+(0.22 \pm 0.09)$ fm using $a_m = 0.52$ fm and $+(0.20 \pm 0.09)$ fm using the best fit a_m value. Such values agree well with published values for tin.[19]

The real- and imaginary-potential shapes obtained for the best fits with the folding model are included in Fig. 2. The real potentials of the folding model are all characterized by a reduced magnitude, compared to the standard model, around the halfway points of the potential with greater magnitude at the origin. The tails of the potentials are similar with the two models.

The ratio of the folded strength for the final fit, V_{RFO}, to that predicted using the nucleon-α potential strength is included in Table I. For ^{45}Sc (7%) and ^{65}Cu (19%) significant increases are found; for ^{90}Zr (1.7%) and ^{122}Sn (−0.5%) little change occurs. However, in view of the uncertainties in the precise shape of the nuclear-matter distribution, none of these is considered to be a serious departure from a simple folding model using a free nucleon-α-interaction real potential.

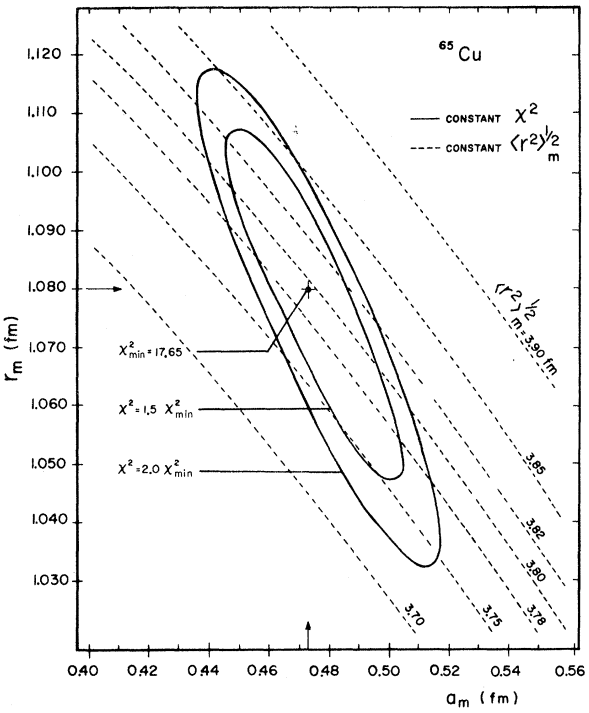

FIG. 5. Contour plots of equal χ^2 values using the folding model and the ^{65}Cu$(\alpha,\alpha)^{65}$Cu data. The contours were determined by finding χ^2 minima with variation of V_{RFO}, W_V, r_I, and a_I for various combinations of r_m and a_m.

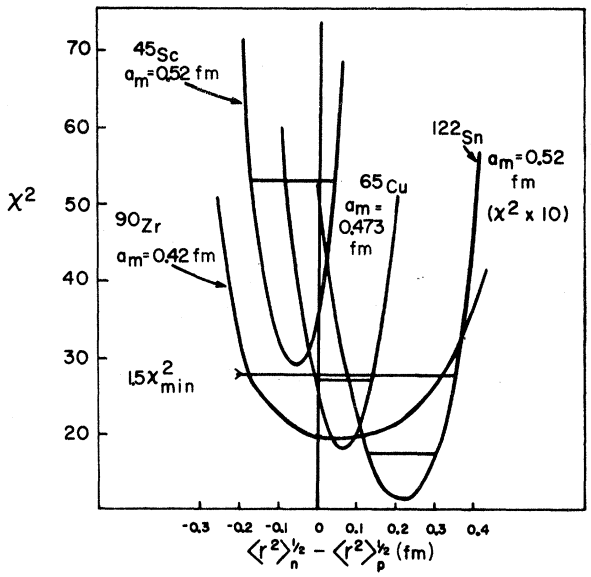

FIG. 6. χ^2 variation for α-nucleus elastic scattering data as a function of $[\langle r^2\rangle_n^{1/2} - \langle r^2\rangle_p^{1/2}]$ for the different cases using the folding model. These plots were obtained by finding minimum χ^2 values when searching on V_{RFO}, W_V, r_I, and a_I for a range of values of r_m, with a_m fixed at the values shown.

IV. DISCUSSION

It has been shown that a nucleon-α interaction can be chosen which simultaneously gives a good representation of free nucleon-^{4}He-scattering data and, when folded with a nuclear-matter distribution, consistent with existing data, also gives a good representation of α-nucleus scattering. Moreover, the fits to both the nucleon-^{4}He and the α-nucleus data are improved over those obtained previously when the interaction was only required to represent one or the other of the types of data. Particularly noticeable is the representation of the α-nucleus scattering data, when compared to those achieved with standard six-parameter phenomenological models, since even a simple four-parameter folding model shows significant improvement. At face value, this suggests that a simple microscopic description of α-nucleus elastic scattering in which the shape of the real potential is obtained from a folding of a free nucleon-α interaction with a nuclear-density function is a good approximation. This implies that additional antisymmetrization and polarization effects due to the binding of nucleons in the nucleus play a relatively minor role in the α-elastic process at these energies and can be accommodated by relatively small adjustment in the over-all strength parameter. If this is correct, the sensitivity of the results to the choice of the matter parametrization makes such measurements a method of obtaining information concerning the tail of the distribution of nucleons in nuclei. This is an attractive conclusion to draw from the results; however, it may be a little premature.

The folded curves of Fig. 1 show clearly that a local-potential representation of the interaction is sufficient to completely describe the present elastic scattering data. No special mechanisms need be invoked to explain the features of the scattering at large angles as have been suggested previously.[4] Thus, while special mechanisms may be in evidence in some cases, such as ^{40}Ca scattering, they are not necessarily the general rule. The shape of the real potential giving the improved representation was obtained by the folding of two Woods-Saxon (or Fermi) distributions. However, there is no *a priori* reason for choosing such a shape either for the nucleon-α interaction, or for the nuclear-matter distribution; the choices are ones of convention and mathematical convenience. Comparison of the potential shapes obtained with the standard optical model and the present folding model (Fig. 2) show relatively small differences in the important surface region for the real potential. The imaginary potentials do show sizable differences, but in both cases the magnitudes are significantly less than those of the corresponding real potentials. Since the imaginary potential used is purely phenomenological and of small magnitude, the variations with change of real-potential shape for a best fit are perhaps not unreasonable.

Further evidence of the sensitivity of the predictions to the detailed shape of the real potential is obtained from comparison with other folded shapes. Thus, the use of a Gaussian instead of a Woods-Saxon shape for the nucleon-α interaction gives inferior fits to both free nucleon-^{4}He and α-nucleus data[6,8] and the use of a previously obtained[14] Woods-Saxon representation of the nucleon-α interaction instead of the present one, also produces inferior results (e.g. χ^2 3 times greater for ^{65}Cu data). It is clearly important to explore fully these sensitivities before unambiguous information can be deduced concerning nuclear-matter distributions, from α-nucleus elastic scattering data. It is, however, encouraging that the present results for matter rms radii are entirely consistent with other measurements.

---

*Work supported in part by the U.S. Atomic Energy Commission, Contract No. AT(11-1)-1265; this is report number COO-1265-125.

[1]J. S. Blair, Phys. Rev. 95, 1218 (1954); 115, 928 (1959).

[2]See for example D. C. Weisser, J. S. Lilley, R. K. Hobbie, and G. W. Greenlees, Phys. Rev. C 2, 544 (1970).

[3]A. Budzanowski, A. Dudek, R. Dymarz, K. Grotowski, L. Jarezyk, H. Niewodniczanski, and A. Strazalkowski, Nucl. Phys. A126, 369 (1969).

[4]T. Honda and H. Ui, Nucl. Phys. 34, 593 (1962); N. Austern and J. S. Blair, Ann. Phys. (N.Y.) 33, 15 (1965); B. Buck, Phys. Rev. 127, 962 (1962); N. S. Wall, in *Proceedings of the International Congress on Nuclear Physics, Paris, 1964,* edited by P. Gugenberger (Centre National de la Recherche Scientifique, Paris, France, 1964), p. 472; M. W. Berry, Proc. Phys. Soc. Lond. 88, 285 (1966); K. W. Ford and J. A. Wheeler, Ann. Phys. (N. Y.) 7, 259 (1959); M. L. Perl, L. W. Jones, and C. C. Ting, Phys. Rev. 132, 1252 (1963); L. Bertorchi and A. Capella, Nuovo Cimento 44A, 481 (1966); 23, 1061 (1962); T. E. O. Ericson, in *Preludes in Theoretical Physics,* edited by A. de Shalit, L. Van Hove, and H. Feshbach (North-Holland, Amsterdam, 1966), p.321; R. Ceulenur, M. Demeur, and J. Reignier, Nucl. Phys. 89, 177 (1966); V. Barger, and D. Cline, Phys. Rev. Lett. 16, 913 (1966); J. Hogaasen Nucl. Phys. A90, 261 (1967); E. B. Carter, G. E. Mitchell, and R. H. Davis, Phys. Rev. 133, B1421 (1964); G. R. Gruhn and N. S. Wall,

Nucl. Phys. 81, 161 (1966); H. J. Kim, Phys. Lett. 19, 296 (1965); H. C. Bryant and N. Jarmie, Ann. Phys. (N.Y.) 47, 127 (1968); A. Bobrowska *et al.*, Nucl. Phys. A126, 361 (1969).

[5]N. K. Glendenning and M. Veneroni, Phys. Rev. 144, 839 (1966); A. M. Berstein, Adv. Nucl. Phys. 3, 325 (1969); A. M. Bernstein and W. A. Seidler, Phys. Lett. 34B, 569 (1971).

[6]A. Budzanowski, A. Dudek, K. Grotowski, and A. Strazlkowski, Phys. Lett. 32B, 431 (1970).

[7]V. A. Madsen and W. Tobocman, Phys. Rev. 139, B864 (1965); D. F. Jackson, Phys. Rev. Lett. 14, 118 (1964); D. F. Jackson and V. K. Kembhavi, Phys. Rev. 178, 1626 (1969).

[8]C. J. Batty, E. Friedman, and D. F. Jackson, Nucl. Phys. A175, 1 (1971).

[9]P. Mailandt, J. S. Lilley, and G. W. Greenlees, Phys. Rev. Lett. 28, 1075 (1972).

[10]G. W. Greenlees, G. J. Pyle, and Y. C. Tang, Phys. Rev. 171, 1115 (1968).

[11]G. J. Pyle, University of Minnesota Williams Laboratory Report No.COO-1265-64, 1968 (unpublished).

[12]D. F. Jackson and C. G. Morgan, Phys. Rev. 175, 1402 (1968); B. Fernandez and J. S. Blair, Phys. Rev. C 1, 523 (1970).

[13]J. S. Lilley, Phys. Rev. C 3, 2229 (1971).

[14]G. R. Satchler, L. W. Owen, A. J. Elwyn, G. L. Morgan, and R. L. Walter, Nucl. Phys. A112, 1 (1968).

[15]G. L. Morgan and R. L. Walter, Phys. Rev. 168, 1114 (1968); G. L. Morgan, Ph.D. thesis, Duke University (unpublished); B. Hoop and H. H. Barschall, Nucl. Phys. 83, 65 (1966); J. R. Sauers, G. L. Morgan, L. A. Schaller, and R. L. Walter, Phys. Rev. 168, 1102 (1968); T. H. May, R. L. Walter, and H. H. Barschall, Nucl. Phys. 45, 17 (1963).

[16]A. C. L. Barnard, C. M. Jones, and J. L. Weil, Nucl. Phys. 50, 604 (1964); J. Sanada, J. Phys. Soc. Jap. 14, 1463 (1959); L. Brown and W. Trachslim, Nucl. Phys. A90, 337 (1967); L. Brown, W. Haeberli, and W. Trachslim, Nucl. Phys. A90, 339 (1967); R. I. Brown, W. Haeberli, and J. X. Saladin, Nucl. Phys. 47, 212 (1963); M. F. Jahns and E. M. Bernstein, Phys. Rev. 162, 871 (1967).

[17]F. D. Becchetti, Jr., M. S. thesis, University of Minnesota, 1968 (unpublished).

[18]The expression for r_{RN} differs from that given earlier in Ref. 9, which contains typographical errors.

[19]G. W. Greenlees, W. Makofske, and G. J. Pyle, Phys. Rev. C 1, 1145 (1970).

[20]H. A. Acker, G. Backenstoss, C. Daum, J. C. Seus, and S. A. Dewitt, Nucl. Phys. 87, 1 (1966).

[21]The nature and model independence of the size parameter obtained from μ-x-ray studies has been the subject of some discussion. In the present work the use of the rms radius is adequate. Further details can be found in R. C. Barrett, Phys. Lett. 33B, 388 (1970), and references contained therein.